JACS
JOURNAL OF THE AMERICAN CHEMICAL SOCIETY

Communication

pubs.acs.org/JACS

Anisotropic Self-Assembly of Gold Nanoparticle Grafted with Polyisoprene and Polystyrene Having Symmetric Polymer Composition

Tatsuhiro Nakano, Daisuke Kawaguchi,[§] and Yushu Matsushita*

Department of Applied Chemistry, Nagoya University, Furo-cho, Chikusa-ku, Nagoya 464-8603, Japan

Supporting Information

ABSTRACT: Methodology to self-assemble metal nanoparticles into three-dimensional mesoscale patterns is a fundamental technique to construct functional materials. Here, we demonstrate that hybridizing an immiscible polymer pair with a metal nanoparticle allows the hybrid to self-assemble in the film, resulting in spontaneous alignment of the nanoparticles at the phase-separated interface formed by the constituent polymers. Organic−inorganic hybrids composed of polyisoprene, polystyrene, and gold nanoparticle were prepared by multistep "grafting-to" method coupled with alkyne−azide click reaction. The polymer composition can be controlled by the feed ratio of gold nanoparticle to azide ligands. The gold nanoparticle hybrid with symmetric polymer composition forms an "alternating lamellar" structure of polyisoprene and polystyrene, where the gold nanoparticles were forced into the phase-separated interfaces.

It is of importance to control the spatial distribution of nanoparticles to construct functional materials such as all-optical storage, photovoltaic and plasmonic devices.[1] Many efforts have been devoted to control the spatial distribution of nanoparticles at the nanometer scale using self-assembly of layer-by-layer of polyelectrolytes,[2−4] synthetic polymers[5−7] and DNA,[8,9] etc. Among these methods, block copolymers have most often been utilized for the fabrication because they form mesoscale three-dimensional ordered structures in bulk so-called microphase-separated structures. The basic manner of using the microphase-separated structures is either to incorporate nanoparticles into microdomains[10−14] or to make them segregated in the phase-separated interfaces.[11,13−16] For the former case, two methods have been employed: one is blending nanoparticles with block copolymers[11−13,17] and another is *in situ* synthesis of nanoparticles in microdomains.[18,19] For the latter case, the selective spatial distribution of nanoparticles near the polymer/polymer interface has been achieved by utilizing interfacial segregation of nanoparticles in microphase-separated structures, which is controlled by the combination of loss entropy and thermodynamic interactions between nanoparticle surface and constituent polymers.[11,13−16] Recently, the segregation of gold nanoparticles (AuNPs) was accomplished in the middle of microdomains using supramolecular block-graft copolymers.[20−22] However, in all cases, block copolymers were used as templates for assembly of nanoparticles without possessing their own ability to self-assemble.

To the contrary, if nanoparticles are able to hybridize with immiscible polymers with more than two components, the nanoparticle−polymer hybrids can be expected to attain the ability to self-assemble into ordered structures with a nanometer scale and their nanoparticles are forced into the phase-separated interfaces without templates. Such hybrids must be similar to multicomponent star polymers which form microphase-separated structures and their junction points align in the interfaces.[23]

Here we demonstrate how to hybridize AuNPs with two immiscible polymers composed of polyisoprene (I) and polystyrene (S) controlling the polymer composition via multistep "grafting-to" methods using amine-thiol ligand exchange and alkyne−azide click reaction. The hybrid comprised of AuNP, I and S (AuNP-IS) with symmetric polymer composition forms a lamellar structure of I and S and the AuNPs are located at the I/S phase-separated interface.

Thiol-terminated polyisoprene (I-SH) and ethynyl-terminated polystyrene (S-yne) with M_w of 55 kDa and 60 kDa, respectively, were prepared by living anionic polymerizations and a subsequent chain end modification. 1-Azidoundecan-11-thiol (Az-SH) was prepared following the previous reports[24,25] and used as a ligand having a clickable site. AuNP capped with dodecylamine ligands were prepared by single-phase approach,[26] whose average diameter is 2.8 ± 0.3 nm evaluated by TEM observation (Figure S1, Supporting Information). The hybridization of AuNP with I and S was conducted as follows. First, the ligand-exchange reaction from dodecylamine to Az-SH was conducted varying the Az-SH/AuNP feed ratio. Successively, I-SH was grafted onto the AuNP surface covered with the mixed ligands of dodecyamine and Az-SH. In this case, dodecylamine is selectively substituted for I-SH due to the difference in the bond strengths of amine-gold and thiol-gold. S-yne was grafted onto the hybrids composed of AuNP and I-SH via alkyne−azide click reaction between Az-SH and S-yne. The crude hybrid products of AuNP-IS were purified by fractional precipitation and preparative gel permeation chromatography (GPC) to obtain AuNP-IS hybrids with no residual homopolymers. The preparation and characterization of AuNP-IS is described in detail in the Supporting Information. The AuNP-IS hybrids were described with φ_s

Received: March 7, 2013
Published: April 24, 2013

   dx.doi.org/10.1021/ja402412q | J. Am. Chem. Soc. 2013, 135, 6798−6801

value, where φ_s is the average volume fraction of the S component determined by ^{1}H NMR and mass densities of I and S.

Figure 1 shows the relationship between Az-SH/AuNP feed ratio and polymer composition in AuNP-IS hybrids. The φ_s value linearly increases with increasing the Az-SH/AuNP feed ratio whereas the overall grafting density(σ) is constant at 1.4 ± 0.1 chains nm^{-2}, that is, independent of the feed ratio. This means that the amount of the grafted I-SH chains can be determined by the amount of the grafted Az-SH, and that the amount of the grafted S chains is also limited by the excluded volume effect of I chains preexisted on the AuNP surface. Picking up the AuNP-IS hybrid with φ_s = 0.48 (AuNP-IS-0.48) as an example, the numbers of the grafted S and I chains are estimated to be 15 each since the surface area of AuNP is calculated to be 24.6 nm^2 based on the average AuNP diameter. Hence, AuNP-IS-0.48 can be regarded as "the two-component 30-arm star copolymers with AuNP as a junction point".

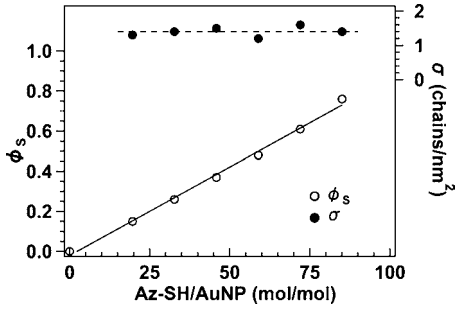

Figure 1. Volume fraction of S (φ_s, ○) and total grafting density of I and S chains on AuNP (σ, ●) as a function of the feed ratio of Az-SH/AuNP. The average diameter of AuNP is 2.8 ± 0.3 nm. The M_ws of I and S are 55k Da and 60k Da, respectively.

The structure of AuNP-IS-0.48 was examined using transmission electron microscopy (TEM) (Figure 2). Figure 2a shows an alternating lamellar structure consisting of I and S phases and having a domain spacing (D) of ~55 nm. Figure 2b represents the enlarged TEM image of AuNP-IS-0.48, where AuNPs are observed as black dots at the interfaces between I and S phases observed as gray and white, respectively. To confirm the spatial dispersion of AuNPs in the film evidently, we observed a nonstained AuNP-IS-0.48 sample by transmission electron tomography (TEMT). A snapshot of the reconstructed TEMT image displays that AuNPs are aligned in the longitudinal direction (Figure 2c), where this observing direction is defined as edge-view. This is consistent with Figure 2a, which shows that AuNPs are forced into the I/S interfaces. On the other hand, a snapshot of the reconstructed TEMT image observed from through-view represents the two-dimensional dispersion of AuNPs with the average nearest neighbor distance of ~15 nm (Figure 2d). Hence, these results clearly demonstrate that the AuNPs are anisotropically distributed at the phase-separated interface in alternating lamellar structures formed by the constituent grafted polymers of I and S onto AuNP.

The structure of AuNP-IS-0.48 in large area was also examined by small-angle X-ray scattering (SAXS). The corresponding 2D SAXS pattern of AuNP-IS-0.48 from edge-view geometry depicts a strong anisotropy shown in Figure 3a. Taking the sector average (azimuthal angle μ = 0 ± 5° and 180 ± 5°) for the AuNP-IS-0.48 with respect to the transverse direction, the integer order peaks were observed (Figure 3b). Note that the intensities of even number peaks are relatively higher than those of odd number ones. This is in stark contrast to the SAXS pattern from lamellar structures of symmetric diblock copolymers showing that the relative intensities of odd number peaks are much higher than those of even number peaks. This result clearly indicates that the regular array of AuNPs in mesoscale leads to the characteristic SAXS profile.

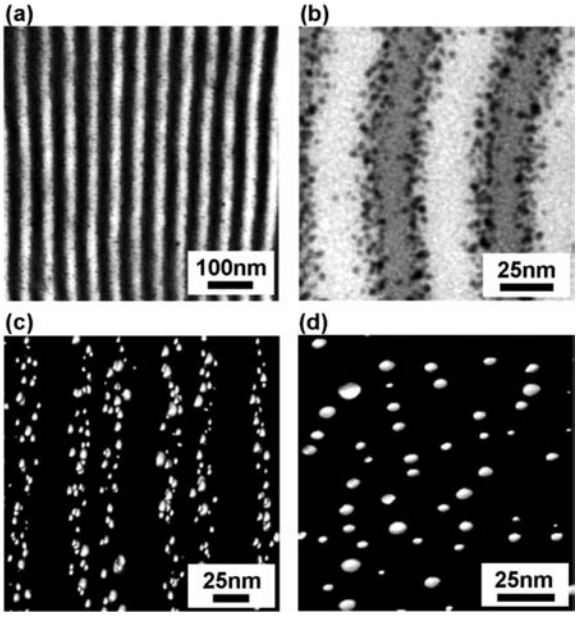

Figure 2. TEM micrographs of solvent-annealed AuNP-IS hybrid film. (a) AuNP-IS-0.48 and b; its magnified one. Since the samples were stained with OsO_4, I and S phases appear dark and bright, respectively. AuNPs appear black dots in b due to the highest electron density among the components. (c and d) reconstructed TEMT images, where the white dots correspond to AuNPs. The observing directions in c and d are defined as edge-view and through-view, respectively. d is obtained by rotating c by 90° about the vertical axis and by extracting the information about the AuNPs distributed in the same plane.

To quantify the structure of AuNP-IS-0.48, the SAXS intensity profile for the transverse direction was analyzed using the paracrystal method.[27−29] The microphase-separated structure of AuNP-IS-0.48 observed from the edge-view direction can be regarded as ABCB four-layer type lamellar structure of an ABC triblock copolymer based on TEM image shown in Figure 2. Assuming that the number of lamellae in a grain is large enough, the SAXS intensity ($I(q)$) of the lamellar structure can be approximated by

$$I(q) \propto P(q)Z(q)q^{-2} \tag{1}$$

where q is scattering vector defined by $q = (4\pi/\lambda)\sin\theta$, λ and 2θ being the wavelength of the X-ray and the scattering angle, respectively. $P(q)$ and $Z(q)$ are the form factor and the lattice factor, respectively. The form factor of the one-dimensional particle of ABCB type lamella ($P(q)_{\mathrm{Lam\_ABCB}}$) is given by[29]

$$P(q)_{\mathrm{Lam.ABCB}} = \iint \left\{ k_1 \frac{\sin(qx/2)}{(qx/2)} \exp\left(-\frac{\sigma^2 q^2}{2}\right) - k_2 \frac{\sin(qy/2)}{(qy/2)} \exp\left(-\frac{\sigma^2 q^2}{2}\right) \right\}^2 \times \exp\left\{ \frac{-[x-(2d_2+d_3)]^2}{2\sigma_x^2} \right\} \exp\left\{ \frac{-(y-d_3)^2}{2\sigma_y^2} \right\} dy dx \tag{2}$$

dx.doi.org/10.1021/ja402412q | J. Am. Chem. Soc. 2013, 135, 6798−6801

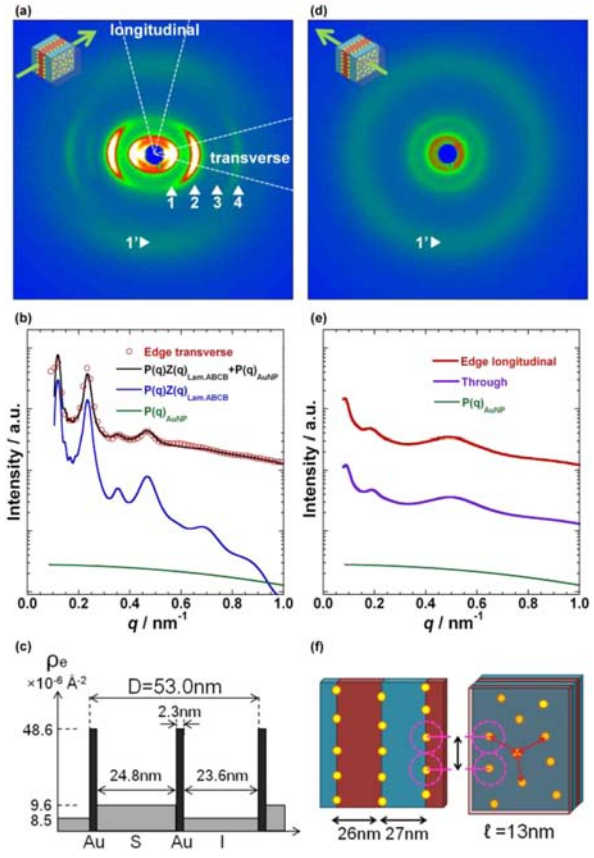

Figure 3. SAXS patterns of AuNP-IS hybrid with φ_s = 0.48. (a) 2D SAXS pattern from edge-view showing an anisotropic pattern. (b) Sector-averaged intensities with the sector angle of ±5° with respect to the transverse direction. In b, the open circles are experimental values and the solid line is calculated one from eqs 1∼7 based on the model 1D electron density profile shown in c. (d) 2D SAXS pattern from through-view shows an isotropic pattern. (e) Comparison of the circular-averaged intensities from d with the sector-averaged ones from a with the sector angle of ±5° with respect to the longitudinal direction. (f) Self-assembled structure of AuNP-IS-0.48.

where d_1, d_2, and d_3 are the thicknesses of I phase, S phase, AuNP phase, and interface, respectively. k_1 denotes the electron density difference between AuNP and I phase while k_2 is that between S and I phases (cf. Figure 3c). σ is related to the interfacial thickness t by the relation, $t = (2\pi)1/2\sigma$. The integration interval is $0-2d_3$ for y and $0-2(2d_2 + d_3)$ for x. The lattice factor for one-dimensional lamellar structure $(Z(q)_{\mathrm{Lam}})$ with domain spacing $(\bar{D} = d_1 + 2d_2 + d_3)$ is given by[27−29]

$$Z(q)_{\mathrm{Lam}} = \frac{1 - |F(q)|^2}{1 - 2|F(q)|\cos(q\bar{D}) + |F(q)|^2} \quad (3)$$

$$|F(q)| = \exp\left(\frac{-g^2\bar{D}^2q^2}{2}\right) \quad (4)$$

$$g \equiv \sigma_D/D \quad (5)$$

where g is Hosemann's g parameter defined by eq 5. σ_D is the standard deviation of D assuming a Gaussian distribution of D. In addition, the scattering from each AuNP also contributes to the total SAXS intensity. The form factor for the AuNP- $(P(q)_{\mathrm{AuNP}})$ is given by

$$P(q)_{\mathrm{AuNP}} = \left[k_3\frac{3}{q^3R^3}[\sin(qR) - qR\cos(qR)]\right]^2 \quad (6)$$

where R is the radius of the AuNP and k_3 is the electron density difference between AuNP and I or S phases. In this case, since the electron density of AuNP is much higher than those of I and S phases, the electron density difference between I and S phases is assumed to be negligibly small. On the whole, the total SAXS intensity $(I(q))$ is given by,

$$I(q) = A \times (P(q)_{\mathrm{Lam,ABCB}} \times Z(q)_{\mathrm{Lam}} + P(q)_{\mathrm{AuNP}}) \quad (7)$$

where A is a scale factor.

The solid line in Figure 3b is calculated from eqs 1−7 and is in good agreement with the experimental values. Hence, it is reasonable to consider that one-dimensional electron density profile shown in Figure 3c reflects the actual concentration profile. The thickness of AuNP phase evaluated by this method is 2.3 nm, which corresponds to the diameter of AuNP. This fact strongly indicates that AuNP aligns at S/I interfaces in a broad range. Furthermore, the thicknesses of the I and S phases are 23.6 and 24.8 nm, respectively, resulting in $\bar{D}$ of 53.0 nm. Hence, SAXS data of AuNP-IS-0.48 are in good agreement with TEM observation.

In contrast to the SAXS pattern from edge-view, the 2D SAXS pattern from through-view shows an isotropic pattern (Figure 3d). Figure 3e shows the circular-averaged SAXS intensities obtained from Figure 3d. A broad peak was observed at around $q \approx 0.5$ nm^{-1}, and the associated correlation length calculated from $d = 2\pi/q$ is 13 nm. This is again in good agreement with the interparticle distance of AuNPs evaluated from the TEM image shown in Figure 2d. Besides, the longitudinal sector-averaged 1D SAXS profile taken from Figure 3a is similar to the circular-averaged SAXS profile from through-view. Hence, these results strongly support the self-assembled structure of AuNP-IS-0.48 schematically shown in Figure 3f.

In conclusion, we have demonstrated a concept for preparing metal nanoparticle−polymer hybrids composed of AuNP, polyisoprene and polystyrene by multistep "grafting-to" methods and alkyne−azide click reaction. Their polymer composition can be controlled by varying the Az-SH/AuNP feed ratio, where the φ_s value linearly increases with increasing the feed ratio. The AuNP-IS hybrid with symmetric polymer composition forms an "alternating lamellar" structure of I and S phases, where the AuNPs are selectively located at the I/S interfaces because AuNP acts as a pseudojunction point of a multiarm star copolymer. These results constitute an important step toward making functional materials such as plasmonic devices by self-assembly.

■ ASSOCIATED CONTENT

Ⓢ Supporting Information

Detailed synthetic procedures, experimental techniques. This material is available free of charge via the Internet at http://pubs.acs.org.

■ AUTHOR INFORMATION

Corresponding Author

yushu@apchem.nagoya-u.ac.jp

Present Address

[§]Education Center for Global Leaders in Molecular Systems for Devices, Kyushu University, Japan

Notes

The authors declare no competing financial interest.

■ ACKNOWLEDGMENTS

This research was in part supported by the Grant-in-Aids for young scientist (A) (No.22685013) and scientific research (A) (No.22245038) from the Ministry of Education, Culture, Sports, Science and Technology (MEXT), Japan. Small-angle X-ray scattering measurements were carried out at Photon Factory (PF), Institute of Materials Structure Science, High Energy Accelerator Research Organization, Japan (Program No. 2012G628 and 2010G642). We thank Kunihito Koumoto, Chunlei Wan and Keiko Ohta in Department of Applied Chemistry, Nagoya University for helping TGA measurements. We are also grateful to Shigeo Arai and Kohei Matsuoka for the reconstruction of 3D-TEM tomography. D.K. thanks Truong Cao Tue for the valuable discussion.

■ REFERENCES

(1) Schmid, G. *Nanoparticles: From Theory to Application*, Second ed.; Wiley-VCH Verlag GmbH & Co. KGaA: Weinheim, 2010.
(2) Kotov, N. A.; Dekany, I.; Fendler, J. H. *J. Phys. Chem.* **1995**, *99*, 13065.
(3) Fendler, J. H. *Chem. Mater.* **1996**, *8*, 1616.
(4) Hammond, P. T. *Adv. Mater.* **2004**, *16*, 1271.
(5) Bockstaller, M. R.; Mickiewicz, R. A.; Thomas, E. L. *Adv. Mater.* **2005**, *17*, 1331.
(6) Balazs, A. C.; Emrick, T.; Russell, T. P. *Science* **2006**, *314*, 1107.
(7) Haryono, A.; Binder, W. H. *Small* **2006**, *2*, 600.
(8) Alivisatos, A. P.; Johnsson, K. P.; Peng, X. G.; Wilson, T. E.; Loweth, C. J.; Bruchez, M. P.; Schultz, P. G. *Nature* **1996**, *382*, 609.
(9) Mirkin, C. A.; Letsinger, R. L.; Mucic, R. C.; Storhoff, J. J. *Nature* **1996**, *382*, 607.
(10) Bockstaller, M. R.; Lapetnikov, Y.; Margel, S.; Thomas, E. L. *J. Am. Chem. Soc.* **2003**, *125*, 5276.
(11) Chiu, J. J.; Kim, B. J.; Kramer, E. J.; Pine, D. J. *J. Am. Chem. Soc.* **2005**, *127*, 5036.
(12) Lin, Y.; Boker, A.; He, J. B.; Sill, K.; Xiang, H. Q.; Abetz, C.; Li, X. F.; Wang, J.; Emrick, T.; Long, S.; Wang, Q.; Balazs, A.; Russell, T. P. *Nature* **2005**, *434*, 55.
(13) Kim, B. J.; Bang, J.; Hawker, C. J.; Kramer, E. J. *Macromolecules* **2006**, *39*, 4108.
(14) Chiu, J. J.; Kim, B. J.; Yi, G. R.; Bang, J.; Kramer, E. J.; Pine, D. J. *Macromolecules* **2007**, *40*, 3361.
(15) Kim, B. J.; Bang, J.; Hawker, C. J.; Chiu, J. J.; Pine, D. J.; Jang, S. G.; Yang, S. M.; Kramer, E. J. *Langmuir* **2007**, *23*, 12693.
(16) Kim, B. J.; Fredrickson, G. H.; Hawker, C. J.; Kramer, E. J. *Langmuir* **2007**, *23*, 7804.
(17) Yeh, S. W.; Wei, K. H.; Sun, Y. S.; Jeng, U. S.; Liang, K. S. *Macromolecules* **2005**, *38*, 6559.
(18) Hashimoto, T.; Harada, M.; Sakamoto, N. *Macromolecules* **1999**, *32*, 6867.
(19) Sohn, B. H.; Seo, B. H. *Chem. Mater.* **2001**, *13*, 1752.
(20) Zhao, Y.; Thorkelsson, K.; Mastroianni, A. J.; Schilling, T.; Luther, J. M.; Rancatore, B. J.; Matsunaga, K.; Jinnai, H.; Wu, Y.; Poulsen, D.; Frechet, J. M. J.; Alivisatos, A. P.; Xu, T. *Nat. Mater.* **2009**, *8*, 979.
(21) Kao, J.; Bai, P.; Chuang, V. P.; Jiang, Z.; Ercius, P.; Xu, T. *Nano Lett.* **2012**, *12*, 2610.
(22) Thorkelsson, K.; Mastroianni, A. J.; Ercius, P.; Xu, T. *Nano Lett.* **2012**, *12*, 498.
(23) Hayashida, K.; Dotera, T.; Takano, A.; Matsushita, Y. *Phys. Rev. Lett.* **2007**, 98.
(24) Collman, J. P.; Devaraj, N. K.; Chidsey, C. E. D. *Langmuir* **2004**, *20*, 1051.
(25) Ru, X.; Zeng, X. H.; Li, Z. M.; Evans, D. J.; Zhan, C. X.; Tang, Y.; Wang, L. J.; Liu, X. M. *J. Polym. Sci. Polym. Chem.* **2010**, *48*, 2410.
(26) Jana, N. R.; Peng, X. G. *J. Am. Chem. Soc.* **2003**, *125*, 14280.
(27) Sakurai, S.; Okamoto, S.; Kawamura, T.; Hashimoto, T. *J. Appl. Crystallogr.* **1991**, *24*, 679.
(28) Shibayama, M.; Hashimoto, T. *Macromolecules* **1986**, *19*, 740.
(29) Tanaka, Y.; Hasegawa, H.; Hashimoto, T.; Ribbe, A.; Sugiyama, K.; Hirao, A.; Nakahama, S. *Polym. J.* **1999**, *31*, 989.